LA-UR-13-27166
Approved for public release; distribution is unlimited.

Title: Fracture-Permeability Relationships of Utica Shale: Early Results

Author(s): Carey, James W.

Intended for: Report

Issued: 2013-09-16

Fracture-Permeability Experiments with Utica Shale: Early Results

Introduction

In October 2013, we will begin a Los Alamos Lab-funded project on the hydraulic fracturing of shale. The goal is to use unique LANL microfluidic and triaxial core flood experiments integrated with state-of-the-art numerical simulation to reveal fundamental dynamics of fracture-fluid interactions. Our particular focus is on the development of CO_2-based fracturing fluids and fracturing techniques to enhance production, greatly reduce wastewater, while simultaneously sequestering CO_2. Our more general goal is to determine fundamental fracture aperture-permeability relationships and the efficiency of hydrocarbon extraction as a function of fracture characteristics.

Last year, as part of a feasibility study for this new project, Chesapeake Energy Corporation (with assistance from Steve Chipera) provided us with a number of Utica Shale samples in the form of 1" cores. These included vertical and horizontal orientation cores from MG-5778, MG-5919.2, DT-8835.5, DT-8984.74, RU-6963.8, RU-6840.9, KB-8334.7, and KB-8439.94. The samples were cut to approximately 1" length. We found that horizontal core were more difficult to maintain intact.

We conducted several experiments using these cores with our new triaxial coreflood with integrated tomography. The purpose of the experiments was to develop our experimental protocol with the new equipment and to examine fracture-permeability relationships in shale samples that were mechanically damaged in compression. These experiments are preliminary to our hydraulic fracturing study that will begin this fall. Our plans this fall will be to further develop techniques to allow studies involving permeability and hydrocarbon extraction from hydraulically fractured (in tension) shale.

In this brief report, we summarize the preliminary experimental data to illustrate the potential of our instrumentation to explore and develop fundamental properties of hydraulically fractured systems. We begin with a brief description of the experimental facility.

Design of Triaxial Coreflood with Integrated Tomography

In order to directly investigate fracture-permeability relationships, we required an experimental system capable of fracturing rock while simultaneously injecting fluids (Figure 1). The system design had to allow observations by either neutron or x-ray tomography so that we could combine measurement of permeability with determination of fracture geometry (apertures and connectivity).

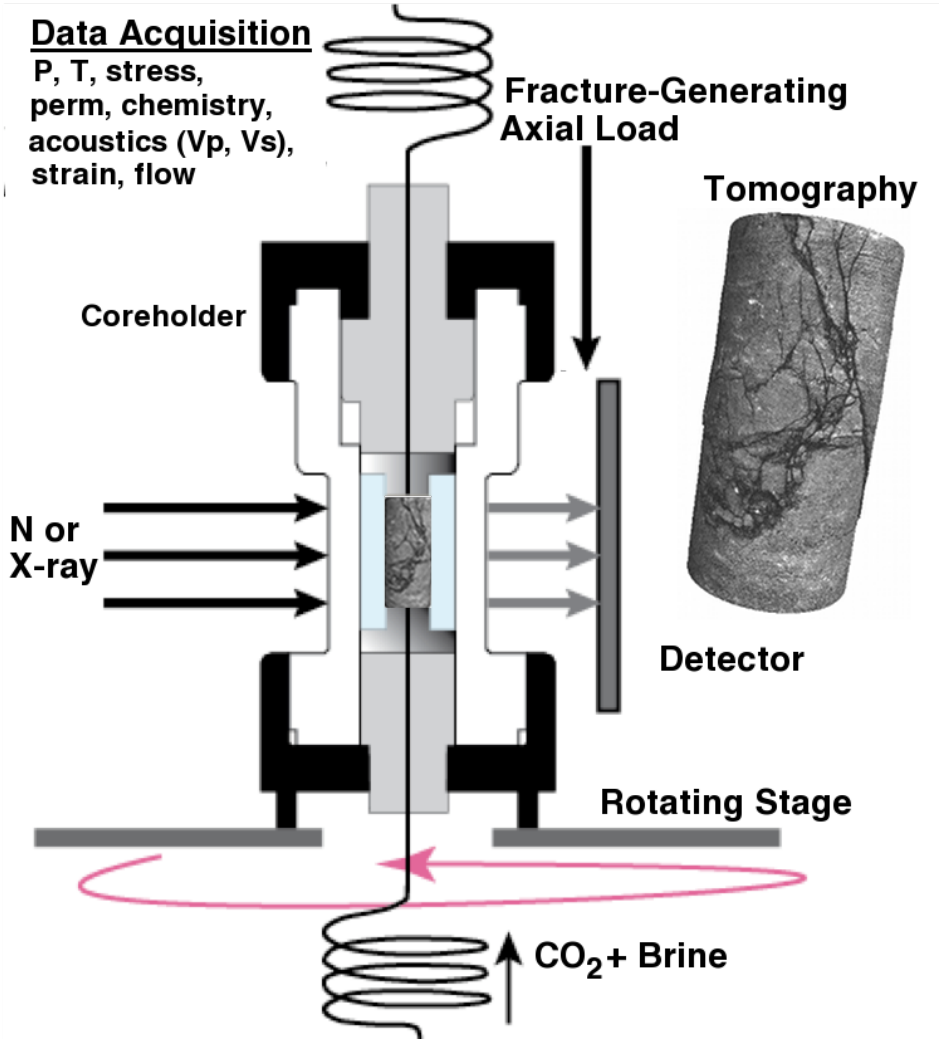

Figure 1. Schematic diagram illustrating the primary components of the multiphase triaxial coreflood laboratory with *in situ* tomography.

We began with a conceptual design (Figure 1) and developed a more complete description of the system performance as follows:

A Multiphase Triaxial Coreflood Laboratory for *In Situ* Tomographic Observation of Fluid Flow and Reaction in Geomaterials Under Stress

Overview of System: A multiphase, tri-axial core-flood system with neutron- and x-ray transparent coreholder for *in situ* tomographic investigations. The system operates at tempertures to 100 ^{o}C and at a confining pressure of 5,000 psi with 5,000-psi pore-pressure delivery. The system allows separate application of confining, axial and pore-pressure and is instrumented to allow measurement of strain and acoustic properties. The fluid delivery system contains an at-conditions fluid sampling port, a high-precision

backpressure regulator, and can make volumetric measurements of fluid outflow.

Detailed System Attributes: The system contains a coreholder, fluid-flow subsystem and tomographic capabilities with features as follows:

1. Core-Holder Design Features
   a. Neutron and x-ray transparent coreholder
   b. Sample size: 1" diameter x 2.5" length
   c. A triaxial load system capable of delivering 500 MPa
   d. Co-injection of two fluids (brine and supercritical CO_2)
   e. *In situ* sensors to include temperature, acoustic velocity, absolute pressure, differential pressure, and axial and radial strain.
   f. External heating system capable of generating 100 ^oC
   g. Data acquisition system (pressure, strain, acoustic velocity, temperature, etc.)
2. Fluid-Flow System Design Features
   a. Isco pumps and accumulators (with flow rates 0.001 to 40 ml/min)
   b. Continuous co-injection of supercritical CO_2 and brine
   c. Fluids heated and mixed prior to injection in core
   d. High quality backpressure regulator with minimal drift
   e. Gas/water meter for CO_2/brine effluent quantification
   f. High accuracy/precision differential pressure measurement across core
   g. Fluid sampling system (prior to BPR at *in situ* experimental conditions)
3. Tomography Design
   a. Moveable coreholder placed on tomographic stage with flexible lines and heating jacket that allows ± 90^o rotation for tomographic imaging while maintaining triaxial stress, confining pressure, temperature and fluid flow conditions.
   b. System is portable to allow temporary installation at tomographic imaging facilities
   c. Tomography beam images a 1x2.5" region at resolutions of 25 μm.
   d. The axial load generated by the triaxial system is occurs by internal hydraulics and does not involve an external load frame

Our research indicates that our system is unique in its ability to fracture rocks at *n situ* conditions while simultaneously making permeability measurements and collecting tomographic images.

Construction of the Multiphase Triaxial Coreflood Laboratory

The triaxial coreflood system was designed at Los Alamos National Lab (LANL). New England Research built the coreholder, and the system was constructed and developed at LANL. It contains a brine and CO_2 fluid delivery subsystem, the

coreholder, measurement equipment, and a large amount of plumbing to connect these components.

In order to provide maximum flexibility for tomographic imaging, the coreflood system was divided onto three mobile carts (Figures 2 and 3). The carts can be loaded on to a truck for transportation and once on site they can be wheeled around to accommodate the requirements of the tomography station. During operation, the carts are connected by high-pressure tubing as indicated in Figure 3.

Figure 2. Photograph of the three mobile carts comprising the triaxial coreflood system. The cart on the right deliver brine (cart 1); the cart on the left delivers CO_2 (cart 2); and the cart in the middle contains the coreholder and pumps for delivering the confining fluid and axial load.

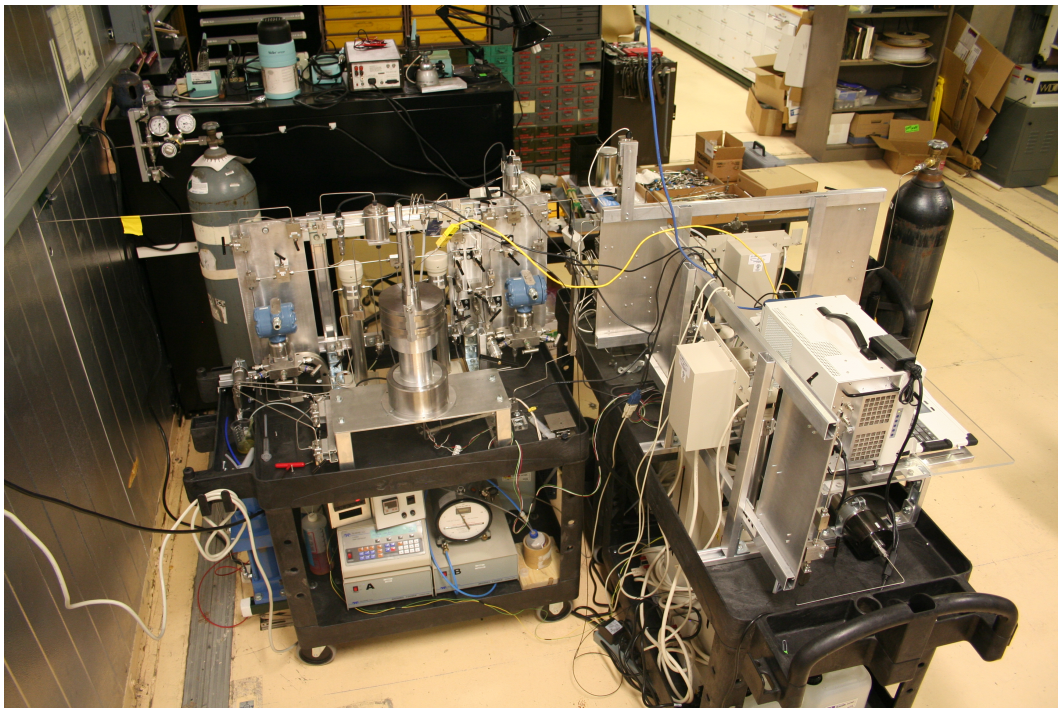

Figure 3. The triaxial coreflood system in an operational configuration. Cart 3 with the coreholder is the focus of the image. The brine cart is in the foreground right and the CO_2 cart is behind the brine cart, facing away from the camera.

The coreholder (Figure 4) can be deployed in either a horizontal or vertical orientation. The coreholder contains mixed-fluid (CO_2+H_2O) inlet and outlet lines, a confining pressure port (we use water as the confining fluid), and an axial pressure line (hydraulic oil). The coreholder is designed to apply an axially symmetric confining pressure and an axial load that uses pistons to squeeze the sample, while injecting the fluids. The unit can monitor sample deformation with strain gauges attached to the sample and/or with a linear variable displacement transducer that measures piston displacement. Acoustic properties (Vp and Vs) are measured with ultrasonic transducers located within the pistons.

During standard laboratory operations, the coreholder sits on a stage on cart 3 (Figure 3 and 4). For *in situ* tomographic operation, the coreholder is placed on a tomographic stage and connected to the coreholder cart via flexible tubing. The instrument is unique in its ability to measure fluid flow and sample deformation while conducting tomographic imaging.

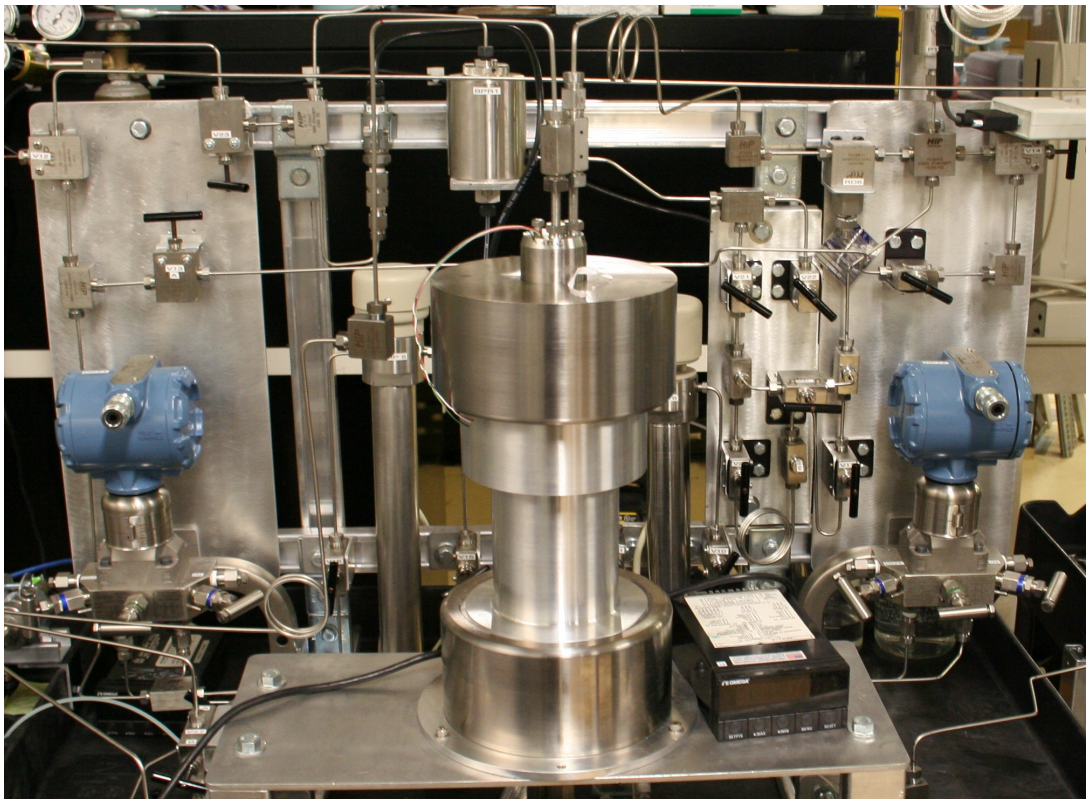

Figure 4. Photograph of the Al-coreholder (cf. drawing in Figure 5). The top of the vessels shows an outlet line for pore fluid; the axial load line, and wires for the acoustic transducer. The center of the coreholder has a decreased diameter of 3.5" to improve tomographic imaging.

Experimental Studies

The focus of the preliminary experimental effort was on the determination of fracture permeability of shale as well as a study of a synthetic wellbore system in shale under reservoir conditions. These measurements require laboratory experiments in which samples are broken at reservoir conditions with simultaneous permeability measurements. Our examination of the literature showed that existing fracture permeability studies utilize samples that are fractured artificially and then placed in the coreflood device for permeability measurement. The problems with this method include the fact that the aperture of the artificial fracture has an unknown relationship to real fractured rock; that the artificial fracture pattern and connectivity may be different from the natural condition; and that handling of the artificially fractured sample will inevitably disturb the fracture.

Our new, triaxial coreflood system has been designed to conduct *in situ* fracturing and permeability measurements of caprock and wellbore materials. However, in order to achieve this goal, we set about conducting a series of increasingly complex

experiments demonstrating instrument functionality but also allowing us to learn and improve experimental protocols.

Experiment with Utica Shale #3 (RU-6963.8, vertical)

The Utica shale is a finely laminated, fossiliferous unit (Figure 55). For this experiment, we demonstrated several new experimental features. We characterized deformation using a linear variable displacement transducer (LVDT), which monitored piston displacement and thus axial deformation of the sample. We also conducted the experiment at supercritical temperature and pressure (45 ^{o}C and 1,200 psi) and determined permeability by injection of supercritical CO_2. All of the data was logged, and we developed plotting tools to facilitate analysis and comparison of the experimental results.

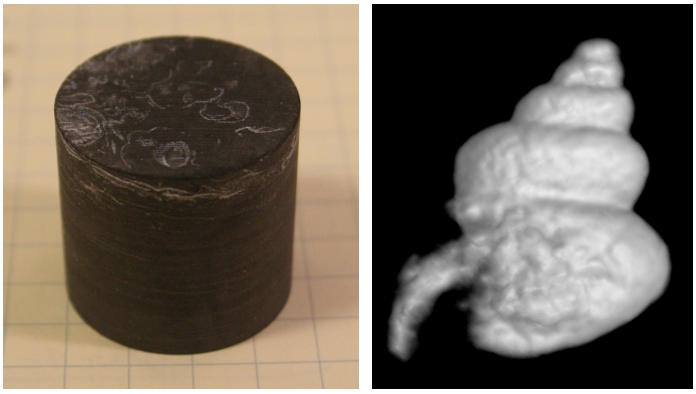

Figure 5. Photograph (left) of Utica shale sample #3 (1" diameter core). The unit is fossilerfous as seen by white traces on the surface of the core (left) and in the tomographic image on the right. The snail-like fossil is about 2.5 mm across.

An overview of the geomechanical data is shown in Figure 6. The experiment was conducted by first loading the sample into the coreholder and filling the confining space with water. We then raised the temperature to 45 ^{o}C and allowed the system to equilibrate overnight. In the second stage of the experiment, the confining pressure and axial pressure were stepped up to the design conditions of 1,700 psi and 2,750 psi, respectively (between about 30,000 and 36,500 s). Although the confining and axial pressures are different, they act over different areas and the net result of these conditions is hydrostatic on the core (i.e., the effective radial and axial stress is the same on the core).

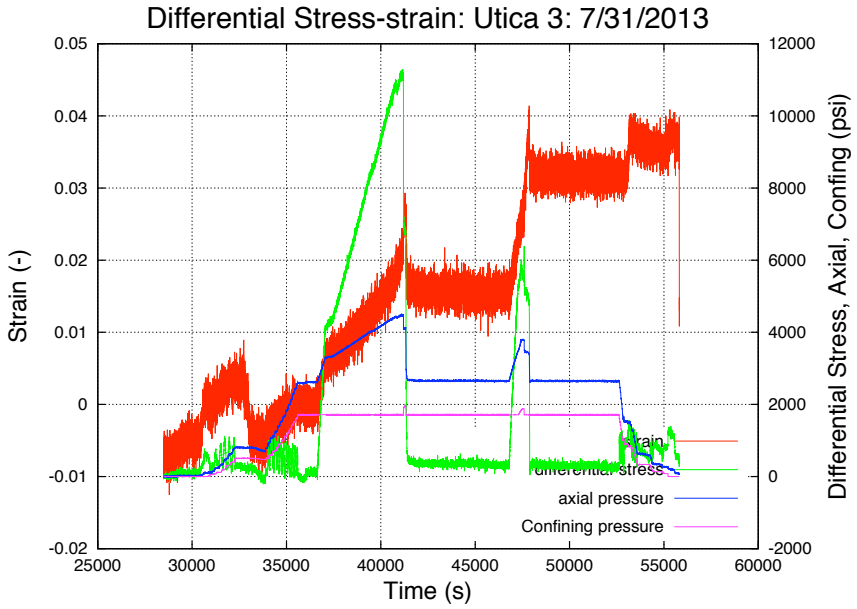

Figure 6. Plot primary geomechanical parameters during the Utica 3 experiments showing strain (as measured by and LVDT, the axial pressure, the confining pressure, net pressure on the sample (differential stress)

In the third stage of the experiment (about 37,000 to 41,000 s), the axial pressure was increased continuously by running the axial load pump at a low constant flow rate. This resulted in the application of a non-hydrostatic axial load ("differential stress" in Figure 6) that increased to 11,000 psi at which point the sample fractured. We observed this as a sudden spike in the strain (positive strain = shortening of the sample), a spike in the confining pressure (as the sample expands into the confining fluid space), and a sudden loss of axial pressure (as the sample shortens).

In the fourth stage of the experiment (about 41,000 to 47,500 s), the axial pressure was returned to hydrostatic conditions (2,750 psi) and a series of permeability measurements were made (Figure 7). Prior to the sample fracturing, a pressure drop of 1,200 psi was maintained across the core without any fluid communication (effectively impermeable). After fracturing, supercritical CO_2 was able to migrate through the core, but still at quite small rates ranging between 40 and 110 μD (micro-Darcy). The permeability was measured by flow of CO_2 out of the core and through the BPR at atmospheric conditions using a gas meter. The values were variable because of the limited amount of gas flow.

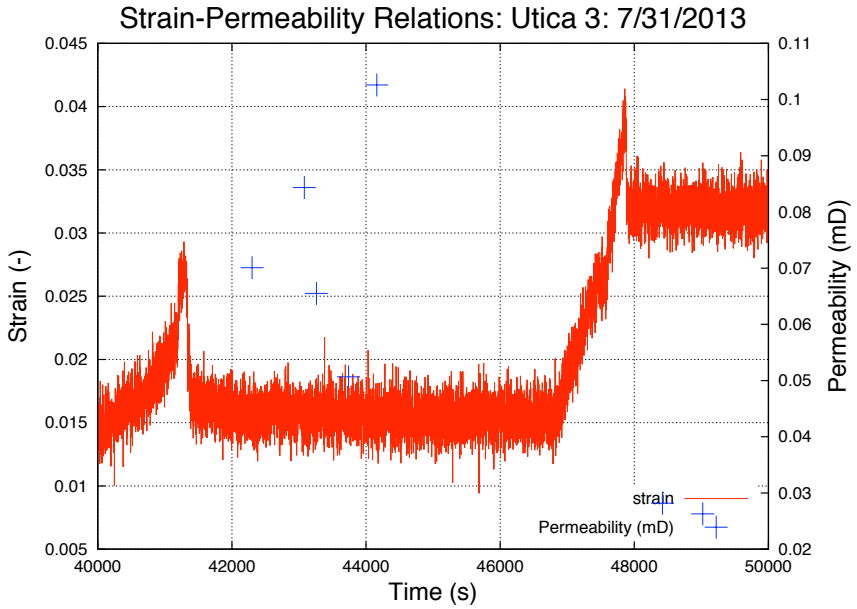

Figure 7. Strain and permeability data for the Utica shale sample #3. The permeability before the sample fractures (at about 41,500 s) was non measureable. The values between 42,000 and 45,000 s were variable but ranged from 40 to 110 μD. After a second strain event, the permeability fell further to 20-30 μD.

In a fifth stage of the experiment (at about 47,000 s), the axial pressure was increased again in an attempt to further deform the sample and create enhanced permeability (Figure 6). The sample shortened from 1.5-3.5% (a significant amount of deformation) without any distinct fracture events. Nonetheless, permeability measurements after the sample was returned to hydrostatic conditions were even lower than before at 20-40 μD. Apparently, the additional strain had sheared-out some of the fractured pathways.

Following the experiment, we conducted x-ray tomography of the shale (Figure 8). The sample was very strikingly fractured, forming a double-cone fracture pattern (conjugate fractures that separated the sample into two distinct cones). These very large fracture patterns are not consistent with the low permeability measured during the experiment (Figure 7). There are several possible reasons for this that are the subject of ongoing investigation. As shown in the subsequent experiments

described below, this occurred in most of the experiments we conducted.

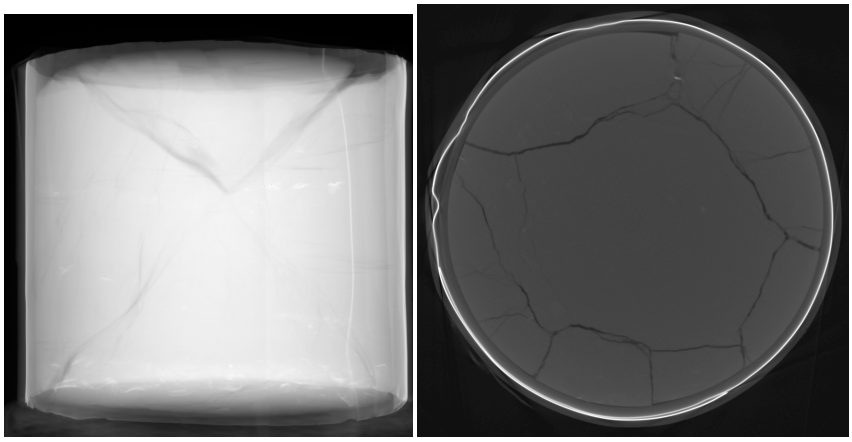

Figure 8. Post-experiment x-ray tomography of Utica shale sample #3. On the left is a radiograph of the sample (1" diameter) showing a beautiful set of conjugate fractures forming a double-cone failure. On the right, a slice through the sample shows an irregular circular fracture pattern with branches to the edges.

Experiment with Utica shale Q (MG-5878)

In a third Utica shale experiment, we used strain gauges and a different strain-stress history to further characterize shale fracture behavior. An experiment overview is shown in Figure 9. After equilibrating the sample at 45 ^{o}C, 1,700 psi confining pressure, we began to steadily ramp up the axial (and differential) pressure until the sample failed at a differential stress of about 13,000 psi. An abrupt increase in the strain was clearly evident corresponding to a distinct fracture event. We then maintained the axial load at about 6,000 psi and monitored deformation. The sample continued to deform, exhibiting plastic, as opposed to brittle, behavior. Permeability, which was initially unmeasurable, rose to about 100 μD.

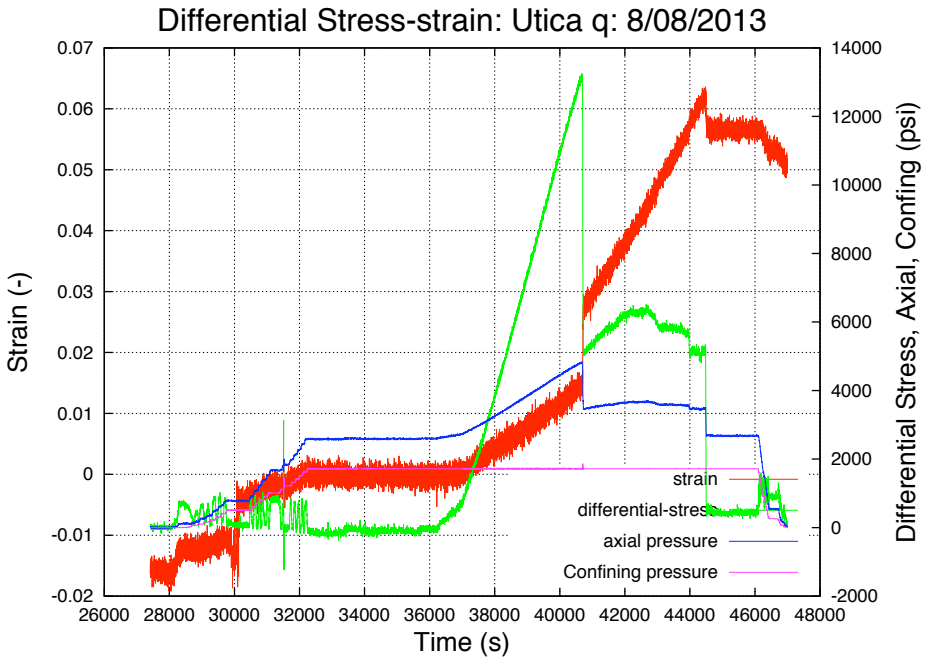

Figure 9. Stress and strain for an experiment with Utica shale (sample Q). After equilibration of the sample at hydrostatic conditions of 2,750 axial pressure (1,700 psi confining), the differential stress was raised continuously until sample failure at about 13,000 psi. Then a lower differential stress was applied which resulted in continued deformation (shortening) of the shale.

This experiment included the use of an axial and radial strain gauge (Figure 10). The gauge was epoxied directly to the core and covered with epoxy and enclosed within a Teflon sleeve. This was our first successful, fluid-tight design (no confining fluid leaked into the core and no supercritical CO_2 escaped from the core into the confining space). However, we did not adequately cover the gauge with epoxy, which compromised the quality of the strain gauge data. In Figure 11, we compare axial strain obtained with the LVDT with the strain gauge data. The radial gauge provides noisy, irregular data until it fails completely at about 31,000 s. The axial gauge shows reasonably well-behaved data from the start until about 30,500 s where it too fails. Until this point, the axial strain gauge data and the LVDT are in reasonable agreement (compare the slope and change in values, rather than the absolute numbers). This promising result will serve as the basis for our ongoing efforts to perfect the full data collection capabilities of the instrument.

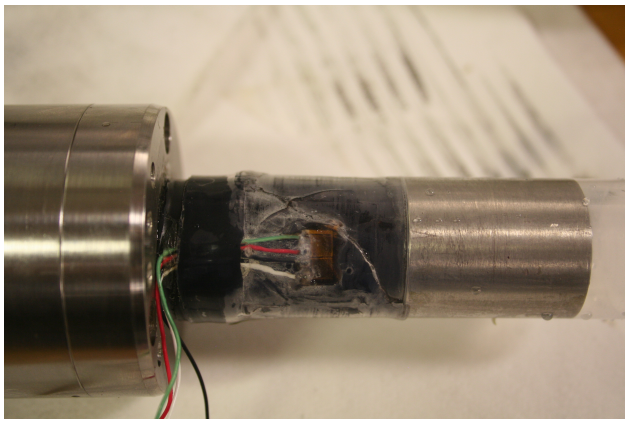

Figure 10. A view of the strain gauge used in the Utica shale "Q" experiment. The strain gauge is below a sleeve of Teflon. The shale sample shows clear evidence of fractures. The metal plug on the right is a spacer.

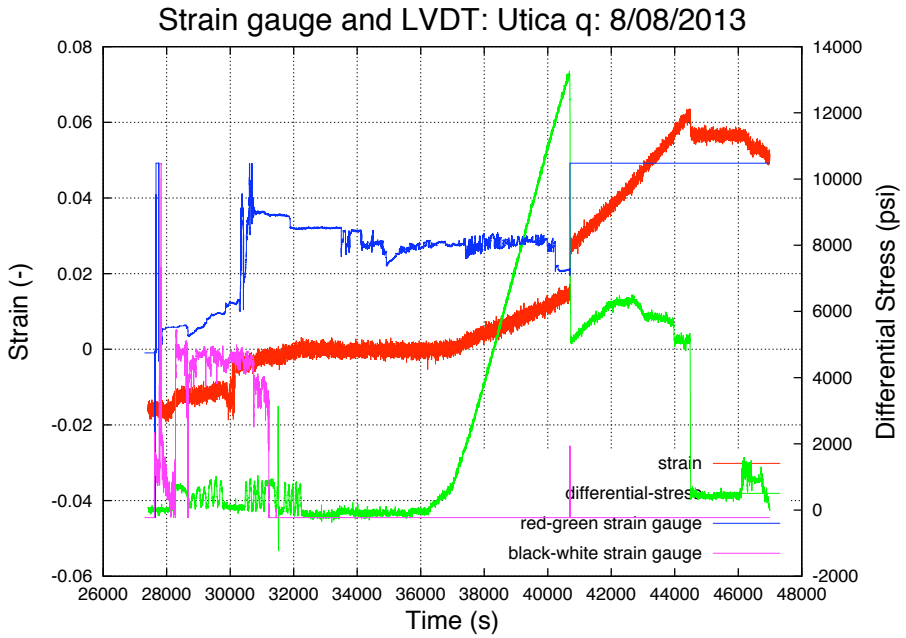

Figure 11. Comparison of strain gauge data with LVDT data on axial strain. The "red-green" gauge is axial; the black-white gauge is radial. The two strain gauges stop functioning after about 31,000 s.

As with the previously described shale samples, post-experiment observations of the core showed an extensive network of fractures (Figure 12). However, these were not sufficient to allow particularly high permeabilities of supercritical CO_2.

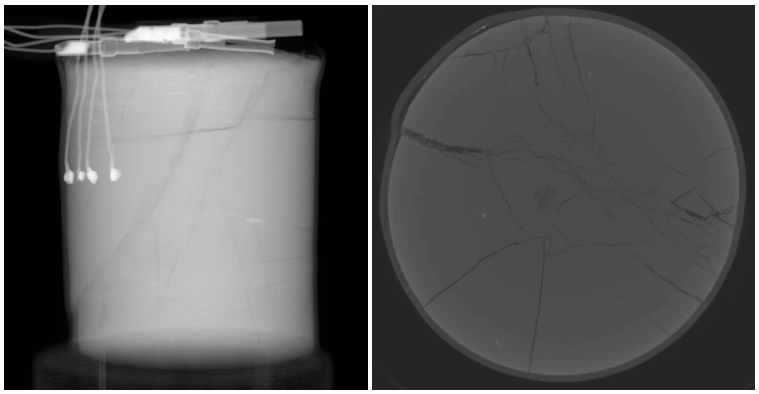

Figure 12. X-ray radiograph and tomographic reconstruction of the Utica shale "Q" experiment. The left shows the strain gauges and an extensive set of fractures, similar to what is observed in the horizontal slice on the right.

Experimental Study of Synthetic Wellbore System

Our previous work has shown that geomechanical damage of wellbore systems is a key vulnerability that can lead to leakage of CO_2 from the storage reservoir. Similar to shale, there have been no studies investigating *in situ*-generated damage-permeability in wellbores. In this study, we created a synthetic wellbore in a shale caprock. We used a 1"-diameter core of Utica shale, drilled a 7/16" hole through, the core, inserted a 3/16"-diameter steel rod, and filled the annular space with type G oilwell cement (Figure 13). The composite material contains all of the key features of a wellbore system: shale, cement, steel, shale-cement interface, and cement-steel interface. The experimental goals were to generate geomechanical stresses, identify which parts of the wellbore system that failed, and determine the permeability of the damaged wellbore.

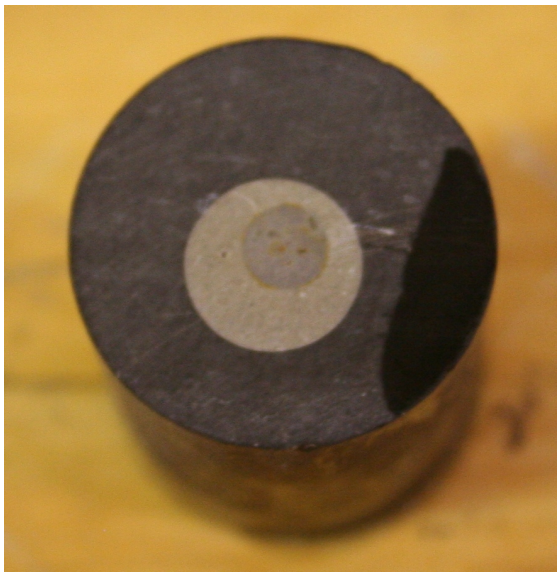

Figure 13. Photograph of synthetic wellbore sample. A 1"-diameter core of Utica shale was drilled through to produce a central channel that was filled with Portland cement and a steel rod.

The synthetic wellbore system was studied at 45 ^{o}C and a confining pressure of 1,700 psi. As with the caprock experiments, the sample was first brought to hydrostatic conditions and then the axial load was increased until sample failure. The initial part of the strain curve shows a discontinuity from 0.01 to < 0.0 (Figure 14). This occurred because we adjusted the LVDT, and the initial part should be ignored. The sample comes to hydrostatic conditions and shows no pressure communication: i.e., the synthetic wellbore is completely impermeable. As the differential stress (or axial load) is increased, the sample deforms until a shortening of just over 3% has occurred where the sample experiences a distinct fracture event at about 42,500 s. However, the permeability of the sample begins to increase at just over 35,000 s and must represent the onset of the development of defects in the wellbore system.

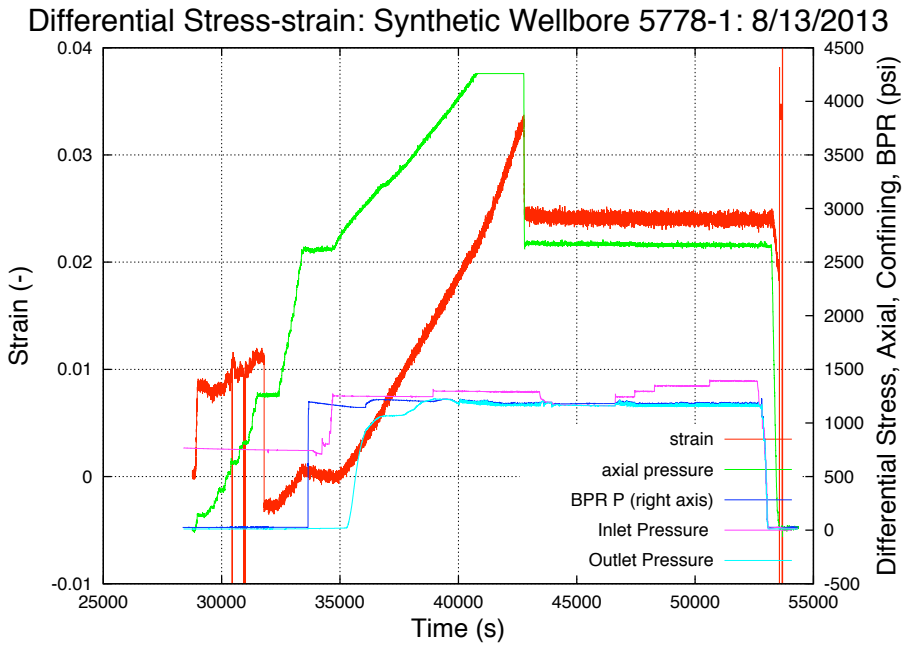

Figure 14. Overview of geomechanical-permeability test of the synthetic wellbore system. The experiment reaches hydrostatic conditions at about 33,000 s. The axial load is then increased from just prior to 35,000 s until sample failure at about 42,500 s. Thereafter, the sample is held at hydrostatic conditions.

The stress-strain behavior of the sample is shown in Figure 15. The strain was measured with an LVDT and represents shortening of the entire composite. The sample fractured at about 2.2% and 9,800 psi, failing to a total strain of about 3.3%. However, earlier in the stress-strain history (0.6% and 3,700 psi), the sample shows a distinct break and reflects a smaller fracture event. Following fracture-failure, the experiment was returned to hydrostatic conditions. The strain recovers only slightly during this period to 2.5%.

The permeability of the wellbore system was measured several times during application of stress and after a return to hydrostatic conditions (Figure 16). Permeability measurements began soon after the outlet pressure reached 1,200 psi, indicating supercritical CO_2 communication across the core. These data were

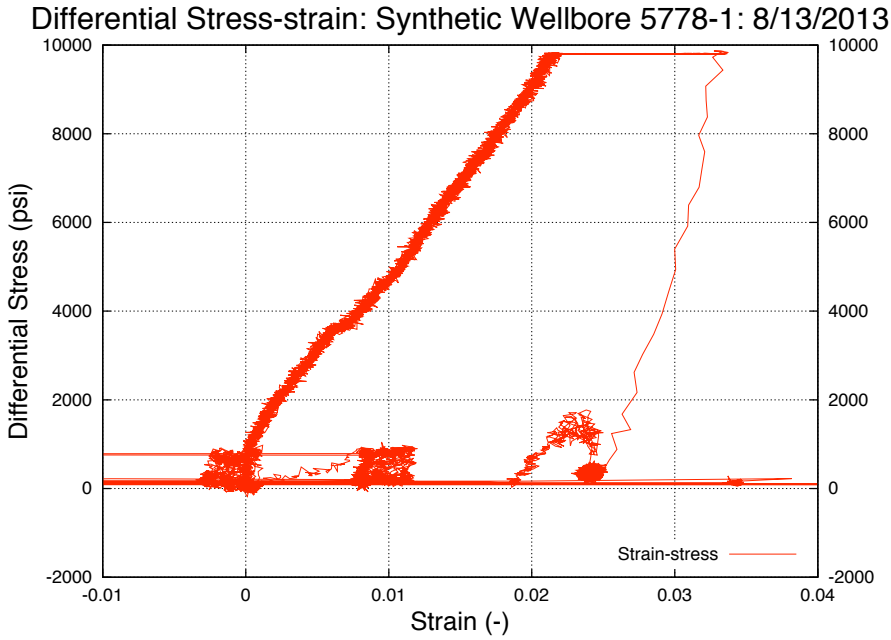

Figure 15. Stress-strain data for the synthetic wellbore. At a strain of ≈2.2%, the sample fractures and shortens substantially to ≈3.3%.

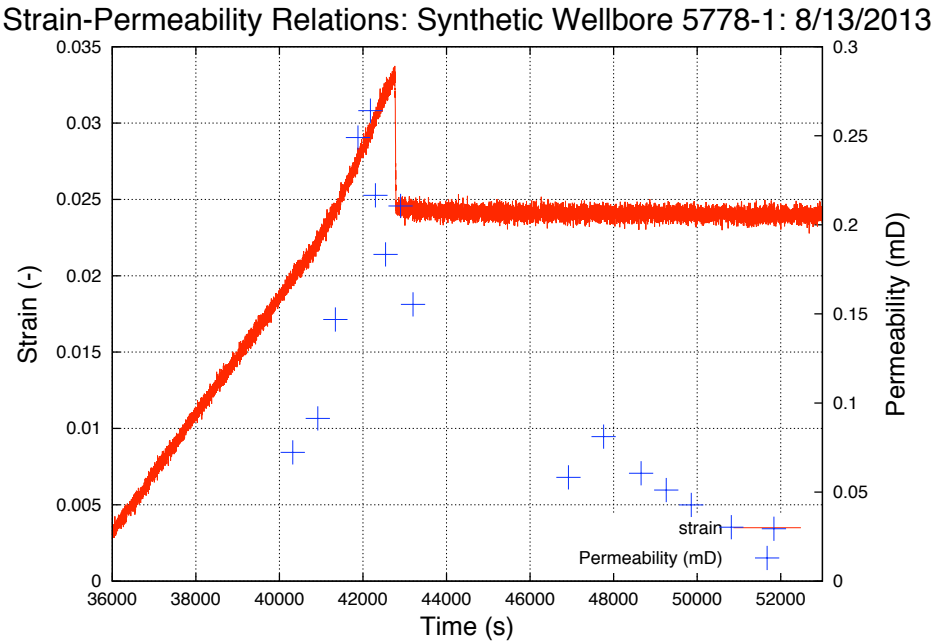

Figure 16. Strain and permeability data for the synthetic wellbore system. The sample had no permeability at the start of the experiment. Permeability increased from 80-200 μD during continuous strain. After the sample fractured, the permeability decreased to 40-80 μD.

collected while the sample was undergoing deformation (continued increase in differential stress), and so these data do not represent steady state values. The permeability increased from unmeasureable to about 80 μD. Further deformation resulted in an increase in permeability to about 250 μD. At this point the sample fractured. The axial pressure was lowered to re-establish hydrostatic conditions and another set of measurements indicated a *loss* of permeability to about 40-80 μD.

In addition to the discreet measurements of Figure 16, we also collected continuous permeability data using the flow-rate of the pumping system (Figure 17). This method requires a period of constant pressure drop across the core (otherwise, the CO_2 pump, which is set at constant pressure, is responding to transient conditions that do not reflect a steady flow rate). These data are quite close to the individual gas-meter values shown in Figure 16. Before the sample fractures, a permeability of about 230 μD is recorded. After the fracture, the permeability drops to about 130 μD, which is independent of the pressure drop across the core.

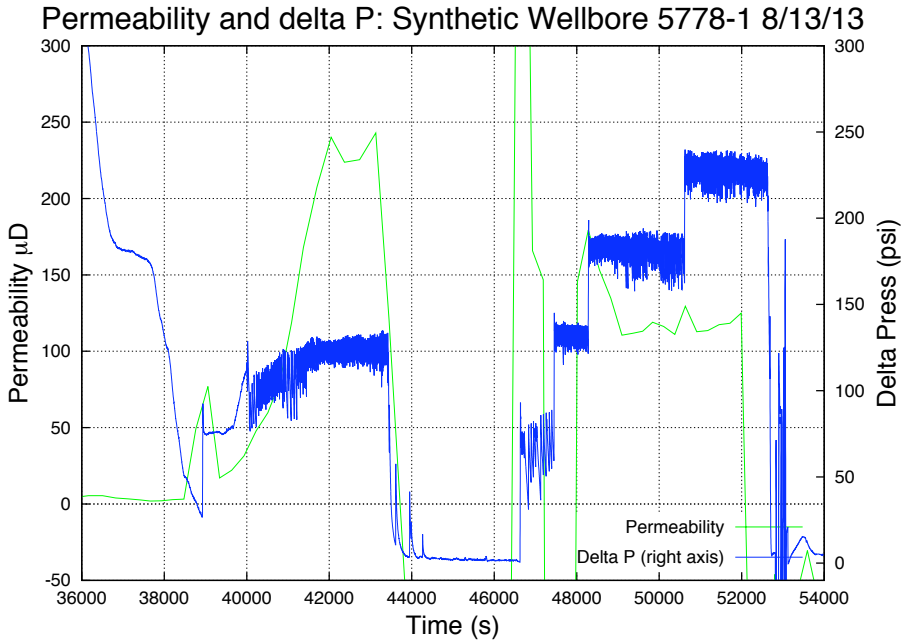

Figure 17. Permeability of the synthetic wellbore systeme measured using the flow-rate of the supercritical CO_2 pumps. Permeability data are reliable only where there is a period of a steady pressure drop (Delta Pressure).

The permeability data indicate that fractures or defects in the synthetic wellbore system developed before the major fracture event at 2.2% strain. These fractures provided a low-permeability pathway that increased as deformation continued. However, when the major fracture event occurred the permeability dropped. This may have happened because large shear movement on the existing fractures created

“fault gouge” that impeded flow. It is also possible that the fracture event relieved stress that was propping open the leakage pathway

X-ray tomography data collected before the experiment are shown in Figure 18. The cement is well formed and continuous within the rock channel. The steel is not centered, which provides some anisotropy to the axial stress. The interfaces between cement and steel or rock appear to be tight. However, there is a pre-existing bedding-plane fracture in the shale.

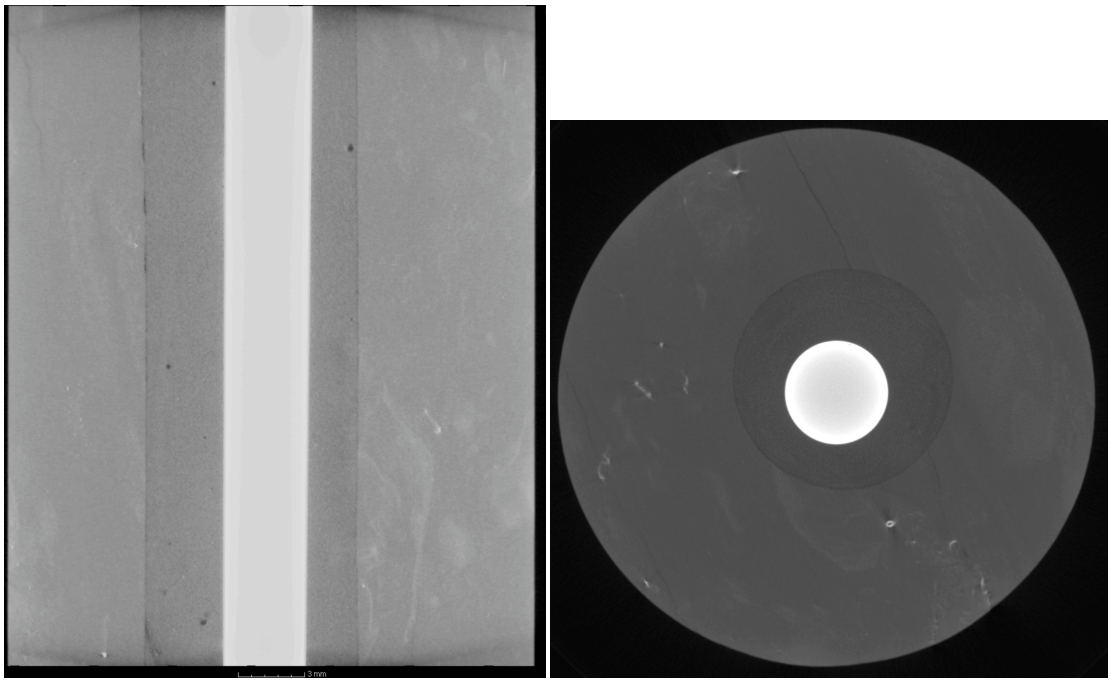

Figure 18. X-ray tomography of the rock-cement-steel synthetic wellbore sample (cf., Figure 13). The cement-rock and cement-steel interfaces are tight and well-formed as seen in a vertical section on the left. A pre-existing fracture in the shale is evident in the cross-section on the right.

Triaxial loading of the synthetic wellbore produced significant fracturing and interface de-bonding (Figure 19). The most striking feature is the formation of extensive bedding-plane fractures in the shale showing that in this experiment damage to the caprock occurs before the cement. In several places the fractures connect with debonded interfaces between shale and cement allowing fluid migration at the cement-shale interface. The cement-steel interface remained undamaged by the experiment and did not generate fluid migration pathways.

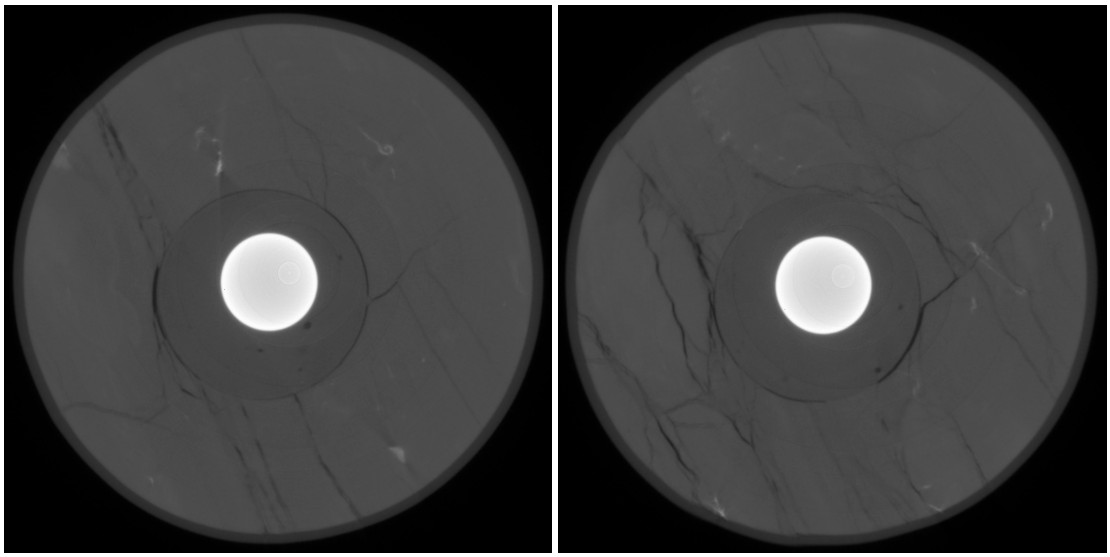

Figure 19. Two cross-sections at different heights obtained by x-ray tomography of the synthetic wellbore system after a triaxial experiment. Both slices show extensive fracturing of the shale, predominantly along bedding planes but also cross-cutting. They also the formation of an interface gap between shale and cement (cf. Figure 18).